Available online at www.sciencedirect.com
ScienceDirect
Journal of Computational Physics 218 (2006) 702–719
JOURNAL OF COMPUTATIONAL PHYSICS
www.elsevier.com/locate/jcp

Linearized perturbed compressible equations for low Mach number aeroacoustics

Jung H. Seo, Young J. Moon *

Department of Mechanical Engineering, Korea University, 1-5 Anam-dong Sungbuk-ku, Seoul 136-701, Republic of Korea

Received 1 November 2005; received in revised form 3 March 2006; accepted 3 March 2006
Available online 19 April 2006

Abstract

For efficient aeroacoustic computation at low Mach numbers, the linearized perturbed compressible equations (LPCE) are proposed. The derivation is based on investigation of the perturbed vorticity transport equations. In the original hydrodynamic/acoustic splitting method, perturbed vorticity is generated by a coupling effect between the hydrodynamic vorticity and the perturbed velocities. At low Mach numbers, the effect of perturbed vorticity on sound generation is not significant. However, the perturbed vorticity easily becomes unstable, and causes inconsistent acoustic solutions, based on grid dependence. The present LPCE ensures grid-independent acoustic solutions by suppressing the generation of perturbed vorticity in the formulation. The present method is validated for various dipole and quadruple vortex-sound problems at low Mach numbers: (i) laminar dipole tone from a circular cylinder at Reynolds number based on the cylinder diameter, $Re_D = 150$ and free stream Mach number, $M_\infty = 0.1$, (ii) quadruple sound of Kirchhoff vortex at Mach number based on the rotating speed, $M_\Theta = 0.1$, and (iii) temporal mixing layer noise at Reynolds number based on the shear layer thickness, $Re_\delta = 10000$ and Mach number based on the shear rate, $M_s = 0.1$.

PACS: 43.28.+h; 47.11.+j; 47.27.Sd

Keywords: Computational aeroacoustics; Low Mach number; Hybrid method; Perturbed compressible equations

1. Introduction

Many industrial flow applications such as automobiles, fans, and etc. operate at low speeds and low aeroacoustic Mach numbers, e.g. $M \leqslant 0.3$. Direct numerical simulation (DNS) of low Mach number aeroacoustics still remains a challenging problem because of scale disparities between the hydrodynamic vortical motions and the acoustic waves. In this regard, a hydrodynamic/acoustic splitting method is considered a good alternative for prediction of flow noise at low Mach numbers.

In previous hydrodynamic/acoustic splitting method [7,17,18], a flow field is obtained by solving the incompressible Navier–Stokes equations, while the acoustic field is predicted by the perturbed Euler equations (PEE)

* Corresponding author. Tel.: +82 2 3290 3358; fax: +82 2 926 9290.
E-mail address: yjmoon@korea.ac.kr (Y.J. Moon).

0021-9991/$ - see front matter
doi:10.1016/j.jcp.2006.03.003

which are derived by subtracting the incompressible Navier–Stokes equations from the compressible ones, neglecting the viscous terms. It is generally known that at low Mach numbers, a flow at mean-state is obtained much faster by solving the incompressible Navier–Stokes equations. Therefore, the hydrodynamic/acoustic splitting method is considered computationally more efficient than the direct numerical simulation as well as the other hybrid methods [3], based on the compressible Navier–Stokes equations. Moreover, computational efficiency can be further enhanced, if grid systems for flow and acoustics are treated separately.

It is important to note that the perturbed Euler equations [7,17,18] are mixed-scales, non-linear equations, in which a coupling effect is allowed between the incompressible flow variables and the perturbed quantities. Through this coupling effect, a non-radiating vortical component, so-called 'perturbed vorticity', is generated in the perturbed system. One of the computational difficulties in the splitting method comes from the fact that this perturbed quantity is only retained in the perturbed system and therefore any backscattering of the compressibility effect onto the incompressible flow is not allowed. Although the role of perturbed vorticity on sound generation is negligible at low Mach numbers, this perturbed quantity can easily become unstable for various reasons and eventually becomes self-excited. As a result, inconsistent acoustic solutions may result from the perturbed Euler equations [15].

The perturbed compressible equations (PCE) proposed by present authors [15] remedy the false generation of perturbed vorticity by handling its generation and diffusion properly, especially when noise source is in the shear flow. In PCE, the perturbed Euler equations are modified by introducing the perturbed viscous stresses in the momentum equations and the perturbed energy equation is formally derived from the compressible thermal energy equation. The PCE has been tested for various applications [12,16], including laminar dipole tone from a circular cylinder at $Re_D = 200$ and $M_\infty = 0.3$. For this problem, the PCE solution was shown to be accurate as the DNS solution [15].

In parallel, computational efficiency and accuracy of the PCE in conjunction with the 'grid-splitting' technique has been investigated [11,15]. The study shows that perturbed vorticity could become unstable, if acoustic grid resolution is not properly used. This is because the length scale of the perturbed vorticity is not comparable to that of acoustic waves but closer to the hydrodynamic vortical scale. Thereby, in some cases, grid-dependent acoustic solutions may result from the falsely resolved perturbed vorticity.

In order to resolve aforementioned matters, the linearized perturbed compressible equations (LPCE), a modified version of the original PCE, are proposed in the present study. In LPCE, generation of perturbed vorticity is firmly suppressed by dropping the non-linear coupling terms that contribute to generate vortical components in the perturbed system. This will exclude errors related to the perturbed vorticity, deliberating the fact that it is not an important acoustic source at low Mach numbers. Through this modification, LPCE solutions can be independent of grid resolution and computational efficiency with the grid-splitting technique can be fully achieved.

The present paper is organized as follows. In Section 2, the perturbed compressible equations (PCE) and perturbed vorticity transport equations are revisited, and the linearized perturbed compressible equations (LPCE) are derived. Numerical schemes and methodologies used in this study are introduced in Section 3. In Section 4, three numerical problems (dipole and quadruple) are tested to validate the proposed LPCE formulation. Finally, concluding remarks are summarized in Section 5.

2. Formulations

2.1. Perturbed compressible equations (PCE)

In the hydrodynamic/acoustic splitting method, the instantaneous total flow variables are decomposed into incompressible and perturbed compressible variables as:

$$\begin{aligned} \rho(\vec{x},t) &= \rho_0 + \rho'(\vec{x},t), \\ \vec{u}(\vec{x},t) &= \vec{U}(\vec{x},t) + \vec{u'}(\vec{x},t), \\ p(\vec{x},t) &= P(\vec{x},t) + p'(\vec{x},t). \end{aligned} \tag{1}$$

The incompressible flow variables describe unsteady viscous flow, while acoustic fluctuations and other compressibility effects are represented by perturbed compressible variables. A hydrodynamic flow field is solved by the incompressible Navier–Stokes equations, while its compressibly perturbed field is calculated by the perturbed compressible equations (PCE).

The perturbed compressible equations are written as:

$$\frac{\partial \rho'}{\partial t} + (\vec{u}\cdot\nabla)\rho' + \rho(\nabla\cdot\vec{u}') = 0, \tag{2}$$

$$\frac{\partial \vec{u}'}{\partial t} + (\vec{u}\cdot\nabla)\vec{u}' + (\vec{u}'\cdot\nabla)\vec{U} + \frac{1}{\rho}\nabla p' + \frac{\rho'}{\rho}\frac{\mathrm{D}\vec{U}}{\mathrm{D}t} = \frac{1}{\rho}\vec{f}'_{\mathrm{vis}}, \tag{3}$$

$$\frac{\partial p'}{\partial t} + (\vec{u}\cdot\nabla)p' + \gamma p(\nabla\cdot\vec{u}') + (\vec{u}'\cdot\nabla)P = -\frac{\mathrm{D}P}{\mathrm{D}t} + (\gamma-1)(\Phi - \nabla\cdot\vec{q}), \tag{4}$$

where $\mathrm{D}/\mathrm{D}t = \partial/\partial t + (\vec{U}\cdot\nabla)$, $\vec{f}'_{\mathrm{vis}}$ is the perturbed viscous force vector, Φ and $\vec{q}$ represent thermal viscous dissipation and heat flux vector, respectively. At low Mach numbers, the perturbed viscous forces can be approximated as

$$f'_{\mathrm{vis},i} = \mu_0 \frac{\partial}{\partial x_j}\left(\frac{\partial u'_i}{\partial x_j} + \frac{\partial u'_j}{\partial x_i} - \frac{2}{3}\frac{\partial u'_k}{\partial x_k}\delta_{ij}\right) \tag{5}$$

by assuming viscosity $\mu \cong \mu_0$ (=constant), and Φ and $\vec{q}$ are expressed as:

$$\Phi = \mu\left(\frac{\partial u_j}{\partial x_k} + \frac{\partial u_k}{\partial x_j} - \frac{2}{3}\frac{\partial u_l}{\partial x_l}\delta_{jk}\right)\frac{\partial u_k}{\partial x_k}, \tag{6}$$

$$q_j = -k\frac{\partial}{\partial x_j}\left(\frac{\gamma p}{\rho}\right). \tag{7}$$

Details of PCE derivation can be found in Ref. [15].

Eqs. (2)–(4) along with the incompressible Navier–Stokes equations are a two-step hybrid method. For low Mach number and non thermally driven flows, $-\mathrm{D}P/\mathrm{D}t$ term on the right hand side of Eq. (4) can be regarded as the only explicit acoustic source term. It is also interesting to note that Eq. (4) can be re-written as a 'Dilatation rate equation',

$$D = -\frac{1}{\rho c^2}\left(\frac{\mathrm{d}P}{\mathrm{d}t} + \frac{\mathrm{d}p'}{\mathrm{d}t}\right) + T, \tag{8}$$

where $D = \nabla\cdot\vec{u}'$ is the dilation rate, $\mathrm{d}/\mathrm{d}t = \partial/\partial t + (\vec{u}\cdot\nabla)$, $T = (\gamma-1)(\Phi - \nabla\cdot\vec{q})/(\rho c^2)$ is the thermal effect term, and the relation of $\gamma p = \rho c^2$ is used. From Eq. (8), one can see that compressibility (or dilation rate) effect is related to the total derivative of the pressure (hydrodynamic and perturbed combined). The PCE solutions were critically evaluated with the DNS and Curle's acoustic analogy solutions for the cylinder dipole tone at $Re_D = 200$ and $M_\infty = 0.3$ [15].

2.2. Perturbed vorticity transport equations

Since perturbed variables in PCE are residuals of the total variables with incompressible components subtracted, they represent not only the acoustic fluctuations but also the other compressibility effects such as coupling effects between the hydrodynamic flow and the perturbed field. One particular component of the perturbed variables related to the consistency of the acoustic solution is perturbed vorticity ($\vec{\omega}' = \nabla\times\vec{u}'$), a 'non-radiating' vortical component generated in the PCE system. This fluctuating quantity becomes unstable for various reasons and generates unwanted errors in acoustic calculations [15]. Here, attention is given to identify the terms associated with production and diffusion of the perturbed vorticity in its transport processes.

In order to derive the perturbed vorticity transport equations, the perturbed momentum equation, Eq. (3) is re-written as

$$\frac{\partial \vec{u}'}{\partial t} + \nabla(\vec{u}'\cdot\vec{U}) + \nabla\left(\frac{1}{2}\vec{u}'\cdot\vec{u}'\right) + (\vec{\omega}'\times\vec{U}) + (\vec{\Omega}\times\vec{u}') + (\vec{\omega}'\times\vec{u}') + \frac{1}{\rho}\nabla p' = -\frac{\rho'}{\rho}\frac{\mathrm{D}U}{\mathrm{D}t} + \frac{1}{\rho}\vec{f}'_{\mathrm{vis}} \tag{9}$$

with mathematical identities,

$$(\vec{U}\cdot\nabla)\vec{u}' + (\vec{u}'\cdot\nabla)\vec{U} = \nabla(\vec{u}\cdot\vec{U}) + (\vec{\omega}'\times\vec{U}) + (\vec{\Omega}\times\vec{u}')$$

and

$$(\vec{u}'\cdot\nabla)\vec{u}' = \nabla\left(\frac{1}{2}\vec{u}'\cdot\vec{u}'\right) + (\vec{\omega}'\times\vec{u}'),$$

and definitions of $\vec{\omega}' = \nabla\times\vec{u}'$ and $\vec{\Omega} = \nabla\times\vec{U}$.

Taking a curl on the left hand side of Eq. (9) yields

$$\frac{\partial\vec{\omega}'}{\partial t} + (\vec{u}\cdot\nabla)\vec{\omega}' + \vec{\omega}'(\nabla\cdot\vec{u}') + (\vec{u}'\cdot\nabla)\vec{\Omega} + \vec{\Omega}(\nabla\cdot\vec{u}') - (\vec{\Omega}\cdot\nabla)\vec{u}' - (\vec{\omega}'\cdot\nabla)\vec{u} - \frac{1}{\rho^2}(\nabla\rho\times\nabla p'). \tag{10}$$

With the incompressible Navier–Stokes equations, the right hand side of Eq. (9) can be re-written as

$$\frac{\rho'}{\rho_0\rho}\nabla P - \frac{\rho'}{\rho}\nu_0\nabla^2\vec{U} + \frac{1}{\rho}\vec{f}'_{\text{vis}}, \tag{11}$$

and the curl of Eq. (11) yields

$$\frac{1}{\rho^2}(\nabla\rho\times\nabla P) + \nabla\times\left(\frac{1}{\rho}\vec{f}'_{\text{vis}} - \frac{\rho'}{\rho}\nu_0\nabla^2\vec{U}\right). \tag{12}$$

Combining Eqs. (10) and (12) and dividing both sides by ρ, one obtains the perturbed vorticity transport equations

$$\frac{\partial}{\partial t}\left(\frac{\vec{\omega}'}{\rho}\right) + (\vec{u}\cdot\nabla)\left(\frac{\vec{\omega}'}{\rho}\right) = \underbrace{\frac{1}{\rho}\left[\underbrace{(\vec{\Omega}\cdot\nabla)\vec{u}'}_{\text{I-a}} + \underbrace{(\vec{\omega}'\cdot\nabla)\vec{u}}_{\text{I-b}}\right]}_{\text{I}} - \underbrace{\frac{1}{\rho}\left[\underbrace{(\vec{u}'\cdot\nabla)\vec{\Omega}}_{\text{II-a}} + \underbrace{\vec{\Omega}(\nabla\cdot\vec{u}')}_{\text{II-b}}\right]}_{\text{II}} + \underbrace{\frac{1}{\rho^3}(\nabla\rho\times\nabla p)}_{\text{III}} + \underbrace{\frac{1}{\rho}\nabla\times\vec{F}_{\text{vis}}}_{\text{IV}}, \tag{13}$$

where $\vec{F}_{\text{vis}} = \left(\vec{f}'_{\text{vis}} - \rho'\nu_0\nabla^2\vec{U}\right)/\rho$.

In Eq. (13), one can clearly see that perturbed vorticity is generated and diffused by source terms on the right hand side through: (i) coupling effects between the hydrodynamic vorticity and the perturbed velocities (terms I and II), (ii) entropy field (term III), and (iii) viscous force (term IV). Term I is related to the three-dimensional effect of vortex stretching: stretching of hydrodynamic vorticity by perturbed velocities (term I-a) and stretching of perturbed vorticity by total velocities (term I-b). Term II represents a more direct coupling between the hydrodynamic vorticity and the perturbed velocities. The convective effect of hydrodynamic vorticity by perturbed velocity is represented by term II-a, whereas term II-b is related to the dilatation rate effect. Term III is not so important for low Mach number, non thermally driven flows and term IV only provides physical diffusion to the perturbed vorticity. In our previous study [15], it was shown that term II-a is the most dominant source term that generates perturbed vorticity and term II-b is considered less important at low Mach numbers.

It is interesting to note that perturbed vorticity is not a 'radiating' acoustic quantity but a 'convecting' hydrodynamic vortical. Its physical meaning represents modification of the hydrodynamic vorticity through interactions between the hydrodynamic vorticity and the velocity fluctuations. At low Mach numbers, the magnitude of the perturbed vorticity is small but, if falsely resolved, it becomes self-excited and grows to affect the acoustic solution. Since term II-a is related to the gradient of hydrodynamic vorticity Ω, perturbed vorticity usually appears at the edge of the hydrodynamic vorticity and its length scale is similar to (or sometimes smaller than) the hydrodynamic vortical scale. Therefore, acoustic grid resolution must carefully be handled in PCE calculation.

2.3. Linearized perturbed compressible equations (LPCE)

The linearized perturbed compressible equations (LPCE) are proposed to secure a stable and grid-independent acoustic solution. Neglecting the second-order, non-linear terms such as $(\vec{u}'\cdot\nabla)\vec{u}'$, the original PCE, Eqs. (2)–(4) can be re-written as:

$$\frac{\partial \rho'}{\partial t} + (\vec{U}\cdot\nabla)\rho' + \rho_0(\nabla\cdot\vec{u}') = 0, \tag{14}$$

$$\frac{\partial \vec{u}'}{\partial t} + \nabla(\vec{u}'\cdot\vec{U}) + \frac{1}{\rho_0}\nabla p' = -(\vec{\Omega}\times\vec{u}') - (\vec{\omega}'\times\vec{U}) - \frac{\rho'}{\rho_0}\frac{\mathrm{D}\vec{U}}{\mathrm{D}t} + \frac{1}{\rho_0}\vec{f}'_{\mathrm{vis}}, \tag{15}$$

$$\frac{\partial p'}{\partial t} + (\vec{U}\cdot\nabla)p' + \gamma P(\nabla\cdot\vec{u}') + (\vec{u}'\cdot\nabla)P = -\frac{\mathrm{D}P}{\mathrm{D}t} + (\gamma-1)(\Phi - \nabla\cdot\vec{q}), \tag{16}$$

with mathematical identity, $(\vec{U}\cdot\nabla)\vec{u}' + (\vec{u}'\cdot\nabla)\vec{U} = \nabla(\vec{u}'\cdot\vec{U}) + (\vec{\Omega}\times\vec{u}') + (\vec{\omega}'\times\vec{U})$ used in Eq. (15). Since the left hand side of Eq. (15) does not generate any vortical component, only the right hand side terms are responsible for the generation of perturbed vorticity. The first two terms, $\vec{\Omega}\times\vec{u}'$ and $\vec{\omega}'\times\vec{U}$ correspond to the dominant source terms (terms I and II) in the perturbed vorticity transport equations and the last two terms are associated with the entropy and viscous effects (terms III and IV).

To show the Mach number dependence of each term, the perturbed momentum and energy equations, Eqs. (15) and (16) are combined into a convective wave equation, neglecting the viscous and thermal effect terms and then a Mach number scaling is conducted. The hydrodynamic variables are scaled by their free stream values: $\rho_0 \sim \rho_\infty$, $U \sim U_\infty$, and $P \sim \rho_\infty U_\infty^2$. For the perturbed variables, a Mach number expansion approach [14,19] is employed; for example, a total velocity u can be expressed as $u = U + Mu^{(1)} + M^2u^{(2)} + M^3u^{(3)} + \cdots$ So, the perturbed velocity, $u' \sim Mu^{(1)}$ and from the linear acoustics, $p' \sim (\rho_\infty c_\infty)u'$ and $\rho' \sim (\rho_\infty/c_\infty)u'$. Time is also scaled by l/c_∞, where l is a reference length scale and c_∞ is the speed of sound.

The convective wave equation is written as

$$\underbrace{\frac{\partial^2 p'}{\partial t^2}}_{\mathrm{O}(M)} + \underbrace{(\vec{U}\cdot\nabla)\frac{\partial p'}{\partial t} + \left(\frac{\partial \vec{U}}{\partial t}\cdot\nabla\right)p'}_{\mathrm{O}(M^2)} \underbrace{- \frac{\gamma P}{\rho_0}\nabla^2 p' + \left(\frac{\partial \vec{u}'}{\partial t}\cdot\nabla\right)P + (\vec{u}'\cdot\nabla)\frac{\partial P}{\partial t} + \gamma\frac{\partial P}{\partial t}(\nabla\cdot\vec{u}')}_{\mathrm{O}(M^3)}$$
$$\underbrace{- \gamma P\nabla\cdot\left\{\left\{(\vec{\omega}'\times\vec{U}) + \nabla\cdot(\vec{\Omega}\times\vec{u}')\right\} + \left(\frac{\rho'}{\rho_0}\frac{\mathrm{D}\vec{U}}{\mathrm{D}t}\right) + \nabla(\vec{u}'\cdot\vec{U})\right\}}_{\mathrm{O}(M^4)} = \underbrace{-\frac{\partial}{\partial t}\left(\frac{\mathrm{D}P}{\mathrm{D}t}\right)}_{\mathrm{O}(M)}. \tag{17}$$

Each term has order of $\rho_\infty c_\infty^3 u^{(1)}/l^2$ (or $\rho_\infty c_\infty^3 U_\infty/l^2$) multiplied by a Mach number to the power denoted in Eq. (17). It is clearly shown that the terms responsible for the generation of perturbed vorticity (i.e. the right hand side in Eq. (15)) have a Mach number dependency $\sim\mathrm{O}(M^4)$, whereas the leading-order terms are $\sim\mathrm{O}(M)$. It is also interesting to note that the only explicit acoustic source term, $\mathrm{D}P/\mathrm{D}t$ on the right hand side of Eq. (17) has the same order as the first term in the convective wave equation, $\partial^2 p'/\partial t^2$.

So, it is evident that the first two terms on the right hand side of Eq. (15) are not so responsible for sound generation at low Mach numbers and thereby one can exclude these to suppress the generation of perturbed vorticity. The third term related to a momentum correction to the perturbed mass can also be neglected at low Mach numbers. The last term (perturbed viscous force) is not necessary any more because there is no generation and diffusion of perturbed vorticity.

With the thermal terms neglected in the perturbed energy equation, a set of linearized perturbed compressible equations (LPCE) is written as:

$$\frac{\partial \rho'}{\partial t} + (\vec{U}\cdot\nabla)\rho' + \rho_0(\nabla\cdot\vec{u}') = 0, \tag{18}$$

$$\frac{\partial \vec{u}'}{\partial t} + \nabla(\vec{u}'\cdot\vec{U}) + \frac{1}{\rho_0}\nabla p' = 0, \tag{19}$$

$$\frac{\partial p'}{\partial t} + (\vec{U}\cdot\nabla)p' + \gamma P(\nabla\cdot\vec{u}') + (\vec{u}'\cdot\nabla)P = -\frac{\mathrm{D}P}{\mathrm{D}t}. \tag{20}$$

Since the curl of the linearized perturbed momentum equations, Eq. (19) yields

$$\frac{\partial \vec{\omega}'}{\partial t} = 0, \tag{21}$$

generation of perturbed vorticity is suppressed in the LPCE formulation: i.e. any further changes (generation, convection, and decaying) of perturbed vorticity in time are prevented. A similar concept has also been used by Ewert and Schröder [3] for deriving the acoustic perturbation equations (APE), in which only the acoustic mode is resolved.

Now, one can use larger normal grid spacings near the wall because LPCE is an inviscid form. It is interesting to note that the total derivative of the hydrodynamic pressure, DP/Dt is considered the only explicit noise source term at low Mach numbers. This result agrees with the Goldstein's generalized acoustic analogy theory [6], which is derived from the linearized Navier–Stokes equations for the 'non-radiating' flow field. Ewert and Schröder [3] also have shown that a dominant acoustic source for flows at an incompressible limit can be represented by the hydrodynamic pressure.

3. Numerical methods

All the governing equations (PCE, LPCE) are non-dimensionalized by a reference length scale, speed of sound c_∞, density ρ_∞, and pressure $\rho_\infty c_\infty^2$, and spatial discretizations are made by a sixth-order compact finite difference scheme [8]. The governing equations are transformed into curvilinear coordinates using a Jacobian transformation and metrics are calculated by the same compact scheme to retain the order of accuracy [20]. Time integration is performed by a four-stage Ruge-Kutta method, and a tenth-order implicit spatial filtering proposed by Gaitonde et al. [5] is used to suppress high frequency errors that might be caused by grid non-uniformity. At the far field boundaries, ETA (energy transfer and annihilating) boundary condition [2] is applied to handle the outgoing acoustic waves.

On the solid surface, a non-slip, adiabatic wall boundary condition is used for PCE:

$$\frac{\partial p'}{\partial n} = 0, \quad \frac{\partial \rho'}{\partial n} = 0, \quad \vec{u}' = \vec{0}, \tag{22}$$

while a slip, adiabatic wall boundary condition is applied to LPCE:

$$\frac{\partial p'}{\partial n} = 0, \quad \frac{\partial \rho'}{\partial n} = 0, \quad \vec{u}' \cdot \vec{n} = 0. \tag{23}$$

In our previous study [15], it was shown that the slip wall boundary condition, Eq. (23) applied to the perturbed Euler equations (PEE) generates excessive perturbed vorticity near the wall due to strong coupling effects and therefore acoustic solution is considerably affected. In LPCE, however, Eq. (23) can be applied without concerning such a matter because generation of perturbed vorticity is suppressed in the formulation. In the following section, this issue will be discussed with illustrations.

4. Computational results and discussion

In this section, three numerical problems are validated for the present LPCE formulation: (i) laminar dipole tone from a circular cylinder, (ii) quadruple sound of Kirchhoff vortex, and (iii) temporal mixing layer noise. Computational issues of PCE and LPCE are also discussed, including generation and stability of perturbed vorticity.

4.1. Cylinder dipole tone

In previous study [15], laminar dipole tone from a two-dimensional circular cylinder was considered to verify the perturbed compressible equations (PCE) at Reynolds number based on the cylinder diameter, $Re_D = 200$ and free stream Mach number, $M_\infty = 0.3$. Accurate acoustic solutions were obtained by PCE and comparisons were made with the DNS and Curle's acoustic analogy solutions. In this study, LPCE is tested for the same problem but at $Re_D = 150$ and $M_\infty = 0.1$ and solutions will be closely compared with DNS and PCE.

For the present case, DNS is conducted for an O-grid ($r/D = 180$) with 181×241 points used in the circumferential and radial directions. The LPCE and PCE calculations are also performed with a grid-splitting

technique for computational efficiency. First, a hydrodynamic flow is solved by the incompressible Navier–Stokes equations (INS) with the same grid (181×241), and then acoustic field is computed by LPCE and PCE with coarse 'acoustic' grid (81×181): a radial spacing of acoustic grid at the wall is four times larger than the hydrodynamic grid. According to a speed-up factor of PCE [15], present calculations (INS with LPCE or PCE) are approximately five times faster than the DNS.

The instantaneous pressure fluctuations, $\Delta p' = (P + p') - \overline{(P + p')}$ computed by each method are presented in Fig. 1. The LPCE solution is in excellent agreement with those of DNS and PCE. The pressure fluctuations along the lines at $\theta = 90°$ and $\theta = 30°$ (wake region) are examined in Fig. 2 and no significant differences are found. The LPCE solutions well coincide with DNS, but PCE shows some oscillations in the near field (wake) at $\theta = 30°$. These oscillations are due to the instability of perturbed vorticty and a full discussion on this issue will follow afterwards.

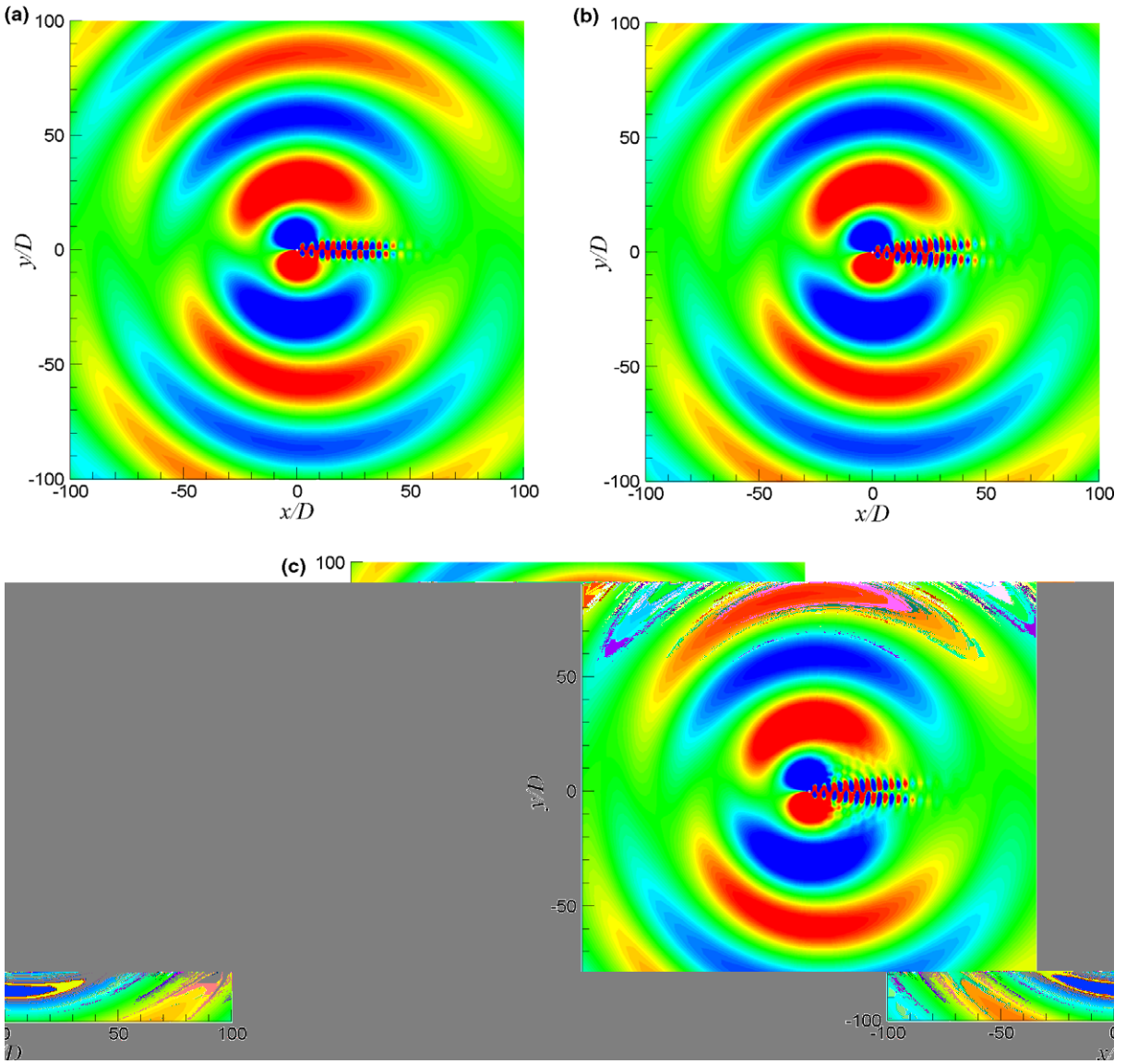

Fig. 1. Instantaneous pressure fluctuation field, $\Delta p' = p - \bar{p}$ for laminar flow past a cylinder at $Re_D = 150$ and $M_\infty = 0.1$; (a) DNS, (b) LPCE, and (c) PCE, 40 contour levels between -2×10^{-5} and 2×10^{-5}, non-dimensionalized by $\rho_\infty c_\infty^2$.

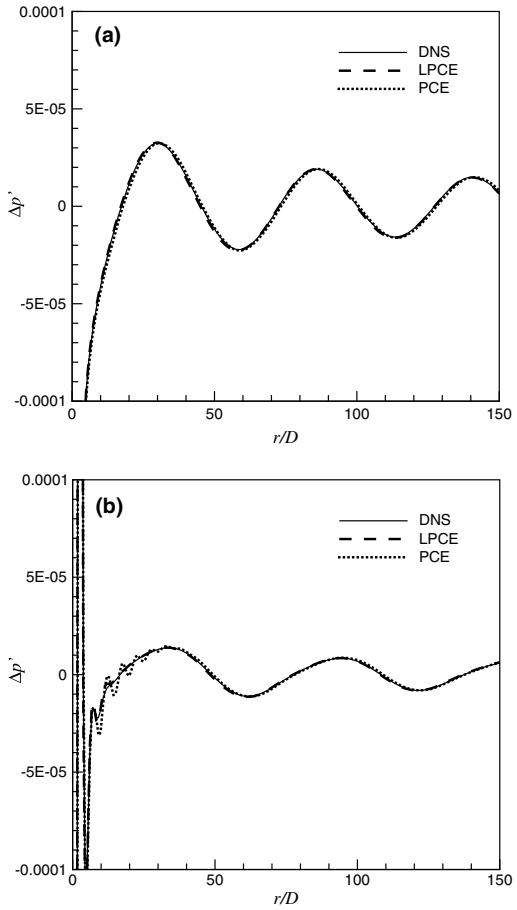

Fig. 2. Comparison of pressure fluctuations along the lines at: (a) $\theta = 90°$ and (b) $\theta = 30°$ (wake region).

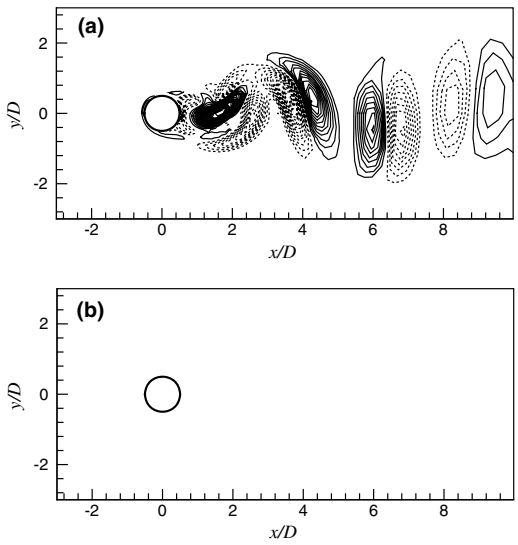

Fig. 3. Perturbed vorticity contours around the cylinder: (a) PCE, (b) LPCE, 40 contour levels between -0.1 and 0.1, non-dimensionalized by c_∞/D.

The perturbed vorticity fields computed by PCE and LPCE are compared in Fig. 3. Fig. 3(a) clearly shows the resolved perturbed vorticity field computed by PCE, while there is no perturbed vorticity generated by LPCE within the same contour range (see Fig. 3(b)). Actually, a peak value of perturbed vorticity calculated by LPCE is 100 times smaller than the PCE result. Even though acoustic far field is well predicted by PCE, a near view of downstream wake region shows spurious generations of perturbed pressure p' (see Fig. 4(a)). These errors are caused by improperly resolved perturbed vorticity in the region, where acoustic grid is too coarse. At low Reynolds numbers, these spurious fluctuations do not severely affect the acoustic field but it can be considerably manifested as the Reynolds number increases. This matter is a very important issue, when one uses a grid-splitting technique. This is because spurious fluctuations can be generated in the perturbed pressure, when perturbed vorticity is not properly resolved with the acoustic grid used. In this regard, present LPCE has an important property that perturbed vorticity does not need to be resolved with the acoustic grid, because its generation is suppressed in the formulation. As shown in Fig. 4(b), one can clearly see that spurious p' fluctuations observed in Fig. 4(a) are not found in the LPCE solution.

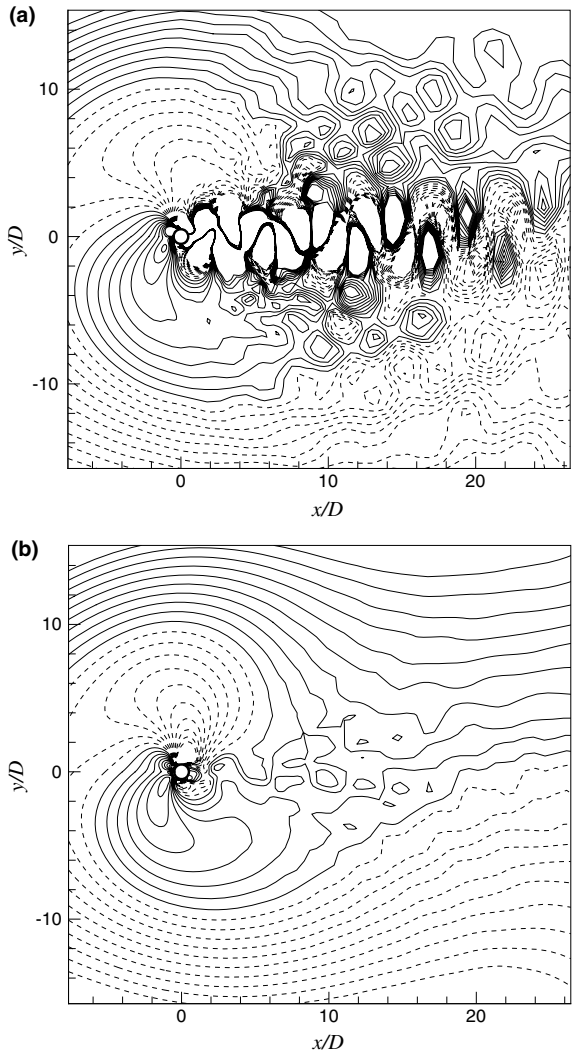

Fig. 4. Perturbed pressure contours in the near field: (a) PCE, (b) LPCE, 20 contour levels between -2×10^{-5} and 2×10^{-5}, non-dimensionalized by $\rho_\infty c_\infty^2$.

As described in Section 2.3, LPCE is an approximation at low Mach numbers and it is important to know the Mach number limit of LPCE. The LPCE is now tested for the present cylinder dipole tone at $M = 0.3$ and 0.5. Comparisons are made in Fig. 5 with the corresponding DNS solutions. At $M = 0.3$, the LPCE solution agrees well with the DNS result, but some discrepancy is observed at $M = 0.5$ due to the neglected coupling terms. This seems consistent with the order analysis described earlier. The relative importance of the neglected terms is proportional to M^3. At $M = 0.3$, the difference between DNS and LPCE is expected to be 0.3^3, or about 3%, which is small enough to be neglected. At $M = 0.5$, however, the difference becomes 12.5% and the computed result shows such a difference in Fig. 5(b). From this test, one can see that the Mach number limit for LPCE lies between $M = 0.3$ and 0.5, but acoustics for $M > 0.3$ do not have to be solved by hybrid methods, rather by DNS.

4.2. Quadruple sound of Kirchhoff vortex

In order to investigate more closely the source of errors caused by falsely resolved perturbed vorticity, a quadruple sound of Kirchhoff vortex is considered. This is a good example that has stiff gradient of hydrodynamic vorticity at the edge of the vortex patch, and therefore pronounced non-linear coupling effects are

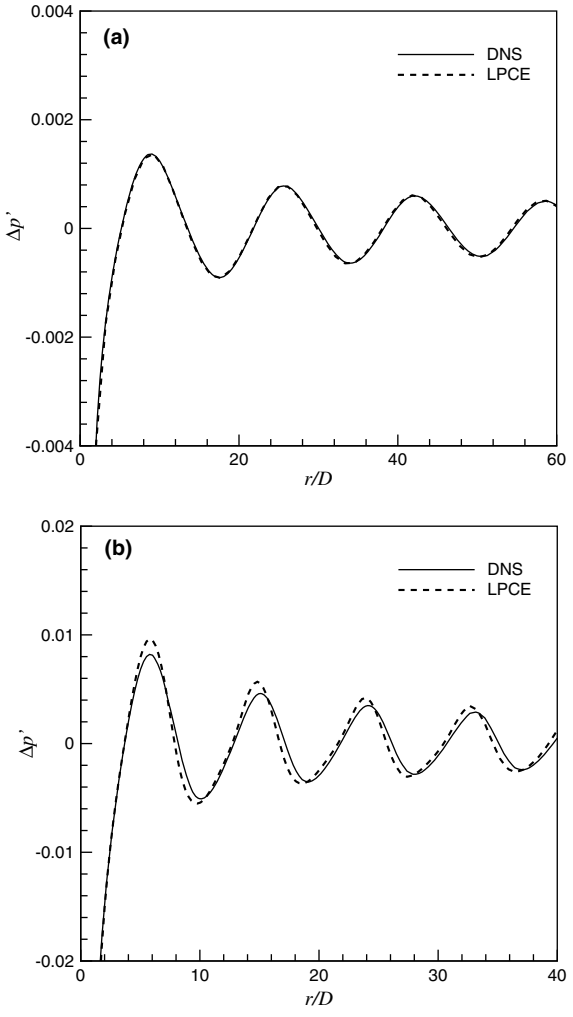

Fig. 5. Comparison of instantaneous pressure fluctuations along the line at $x = 0$ above the cylinder: (a) $M = 0.3$, (b) $M = 0.5$.

expected in acoustic calculation. By rotation of vortex patch, Kirchhoff vortex generates quadruple sound, for which an analytical solution was derived by Müller [13].

The Kirchhoff vortex is a patch of constant vorticity Ω inside an ellipse and zero vorticity outside. A schematic is shown in Fig. 6. The Kirchhoff vortex rotates with a constant angular velocity defined as

$$\Theta = \frac{ab}{(a+b)^2}\Omega,$$

where a and b are the semi-major and -minor axes of an ellipse. The flow Mach number based on a rotating speed is defined by

$$M_\Theta = \frac{(a+b)\Theta}{c},$$

where c is the speed of sound.

For an almost circular vortex case, the semi-major and -minor axes are written as

$$a = \bar{a}(1+\varepsilon) \quad b = \bar{a}(1-\varepsilon),$$

where $\bar{a}$ is a mean radius and $\varepsilon \ll 1$. For this case, an analytical solution for acoustic pressure [13] can be obtained from the Helmholtz equation and is written as

$$p'(r,\theta,t) = Re\left(AH_2^{(1)}(kr)e^{i(2(\theta-\Theta t))}\right), \tag{24}$$

where $H_2^{(1)}$ is the Hankel function of the second order, $k = 2\Theta/c$, and A is defined as

$$A = \frac{4i\rho\bar{a}\varepsilon\Theta^2 e^{-i\pi/2}}{kH_2'^{(1)}(k\bar{a})}. \tag{25}$$

In this study, a quadruple sound of Kirchhoff vortex at $M_\Theta = 0.1$ and $\varepsilon = 0.001$ is computed by LPCE and PCE. The hydrodynamic field is obtained from the exact solution of the incompressible Euler equations [13], and acoustic calculations are conducted for two different grids: the vortex patch is resolved with 100×100 points (fine) and 10×10 points (coarse).

Fig. 7 shows instantaneous pressure fluctuation fields calculated by LPCE and PCE for fine and coarse grids at $t = 500a/c$ (after four rotations of Kirchhoff vortex). The fine grid solutions of LPCE and PCE are

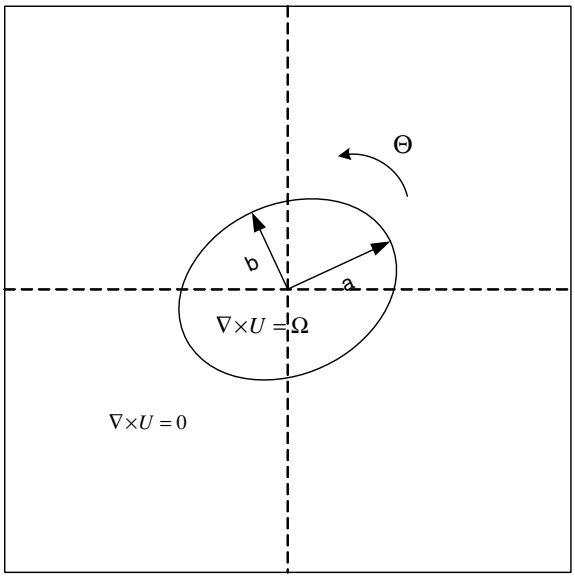

Fig. 6. Kirchhoff vortex.

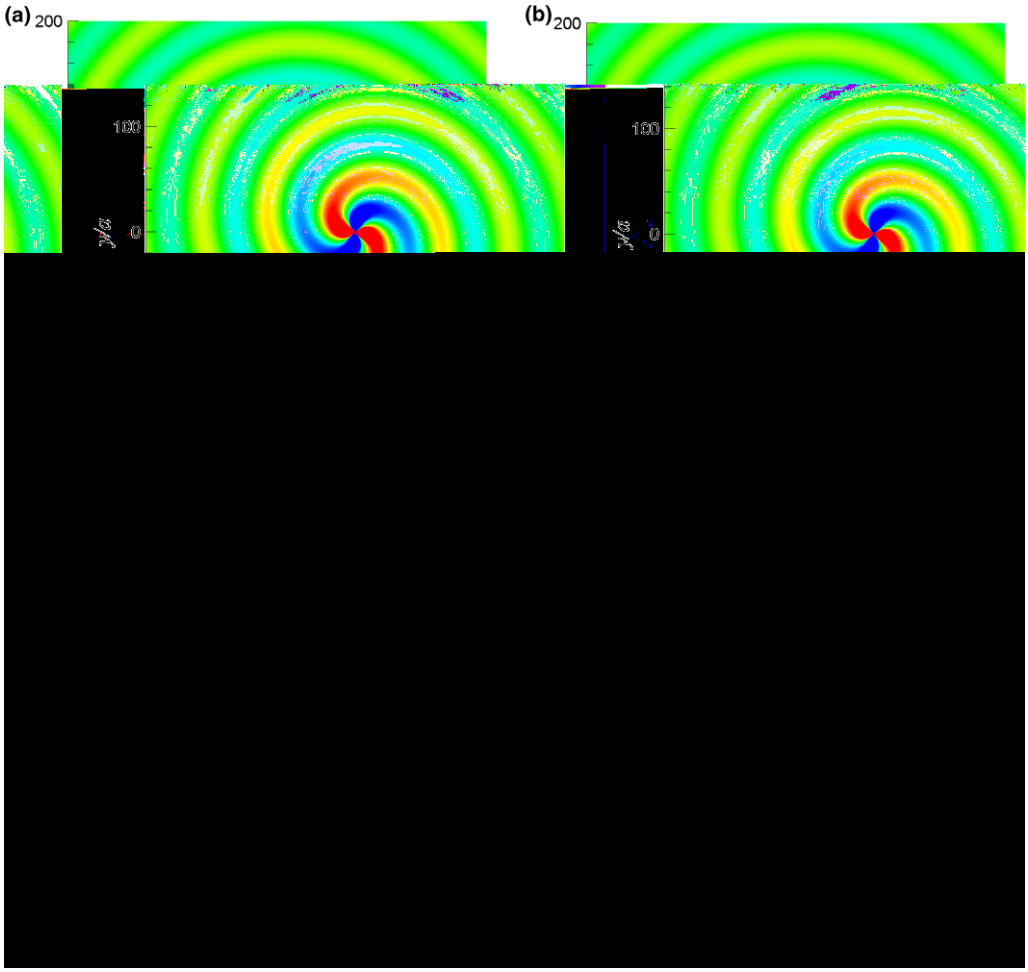

Fig. 7. Kirchhoff vortex sound, instantaneous pressure fluctuation contours: (a) PCE (fine grid), (b) LPCE (fine grid), (c) PCE (coarse grid), (d) LPCE (coarse grid), 40 contour levels between -2×10^{-8} and 2×10^{-8}, non-dimensionalized by $\rho_\infty c_\infty^2$.

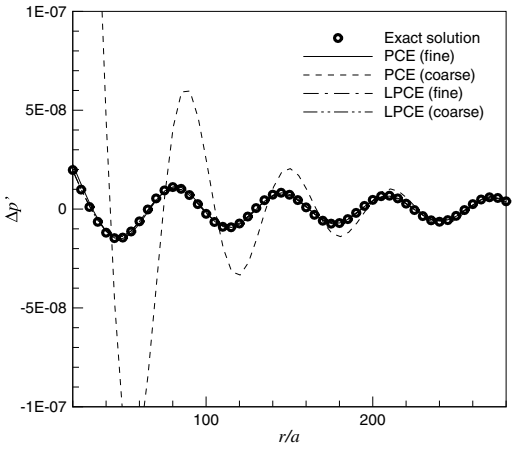

Fig. 8. Comparison of pressure fluctuations along the line at $y = 0$.

almost identical. In comparison with the exact solution, one can clearly see in Fig. 8 that only the coarse grid solution of PCE considerably over-predicts the pressure fluctuations and this is due to the falsely resolved perturbed vorticity, as mentioned before.

Fig. 9 clearly compares the contours of perturbed vorticity computed by PCE for fine and coarse grids. The perturbed vorticity resolved by the fine grid exists only at the edge of the vortex patch, while coarse grid solution shows a largely amplified perturbed vorticity field through the coupling effects. As a result, pressure fluctuation field is also unphysically amplified. On the contrary, LPCE yields a consistent, grid-independent acoustic solution because generation of perturbed vorticity is suppressed in the formulation.

4.3. Mixing layer noise

A two-dimensional mixing layer is considered to investigate the sound field [4] induced by vortex motions (i.e. pairing, co-rotating, and merging) [9]. The hydrodynamic and acoustic computational domains are

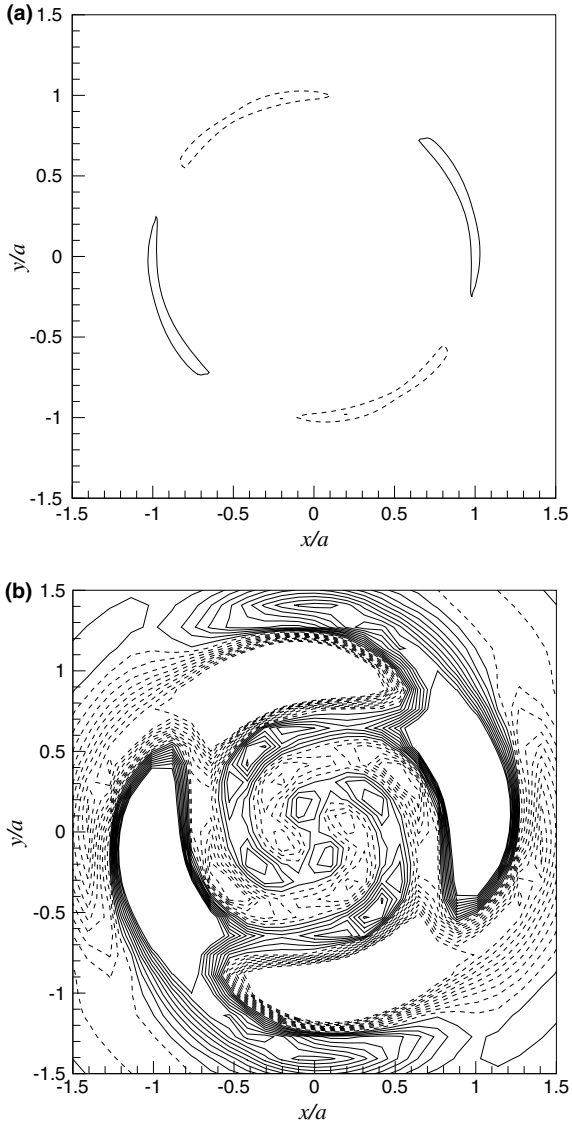

Fig. 9. Perturbed vorticity contours around the Kirchhoff vortex; calculated by PCE: (a) fine grid, (b) coarse grid, 20 contour levels between −0.005 and 0.005, non-dimensionalized by c_∞/a.

schematically shown in Fig. 10, and a periodicity is assumed in the streamwise direction for the domain, $2L$.

An initial condition for the velocities is defined as

$$U_0 = U_\infty \tanh\left(\frac{2y}{\delta}\right) + C_{\text{noise}}\frac{\partial\phi}{\partial y}, \qquad V_0 = -C_{\text{noise}}\frac{\partial\phi}{\partial x}, \tag{26}$$

where a shear layer of thickness, $\delta = L/14$ is perturbed with white noise and $C_{\text{noise}} = 0.001$. A velocity potential for the white noise, ϕ is given by

$$\phi = \exp\left(\frac{-4y^2}{\delta^2}\right)(\sin(8\pi x) + \sin(20\pi x)). \tag{27}$$

A flow Mach number based on the shear rate is $M_s = 2U_\infty/c = 0.1$ and Reynolds number based on the initial shear layer thickness is $Re_\delta = 10{,}000$.

First, evolution of mixing layer is calculated with a hydrodynamic grid (200×200) by the incompressible Navier–Stokes equations. According to the linear stability analysis [1], the most unstable wave length is approximately 7δ [10]. Thus, domain size and initial white noise employed in this study are intended to generate four fundamental eddies (i.e. Kelvin–Helmholtz vortices). The time evolution of hydrodynamic vorticity

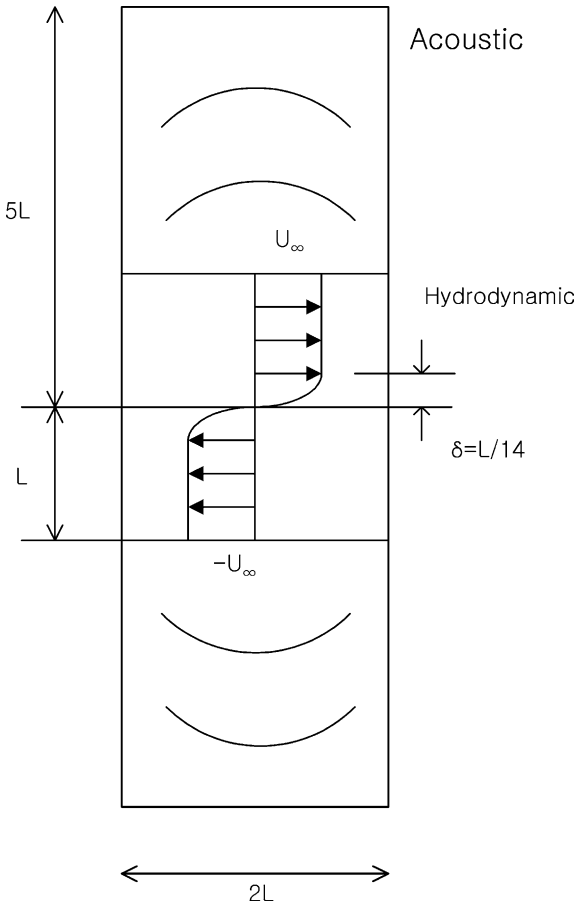

Fig. 10. Schematic of temporal mixing layer noise and computational domain.

is presented in Fig. 11. At $t = 30\delta/U_\infty$, four fundamental eddies appear (first pairing) and they will merge into two eddies (second pairing). Finally, one eddy remains after the third pairing but further development is restricted by the domain size.

The acoustic pulse generated at each pairing-stage is computed by LPCE and PCE with two different grids. The fine grid has the same resolution as the hydrodynamic grid (200×200) for mixing layer ($2L \times 2L$), while only 40×40 points are used in the coarse grid case. Fig. 12 shows the time history of instantaneous pressure fluctuations $\Delta p'$ monitored at $(0, 4L)$. It clearly exhibits the acoustic pulse generated at each pairing-stage as well as the high frequency signals caused by the initial white noise. The PCE calculation with coarse grid yields errors, which are small at early stages but grow in time because falsely resolved perturbed vorticity tends to get self-excited. On the contrary, LPCE solutions are very much grid-independent. In Fig. 13, instantaneous pressure fluctuation fields are compared at $t = 140\delta/U_\infty$. As expected, only the coarse grid solution of PCE is inconsistent with the others. Fig. 14 also shows the perturbed vorticity fields calculated by PCE with fine and coarse grids. As discussed, perturbed vorticity computed by PCE with coarse grid is noticeably different from that with fine grid in structures and scales. Thereby, acoustic field was considerably affected.

In summary, perturbed vorticity is not a major contributor to the generation of acoustic waves at low Mach numbers but can be a source of unwanted errors. Besides, a length scale of perturbed vorticity is usually so small that it is difficult to be resolved with the coarse acoustic grid. By suppressing its generation, present LPCE ensures consistent, grid-independent acoustic solutions at low Mach numbers.

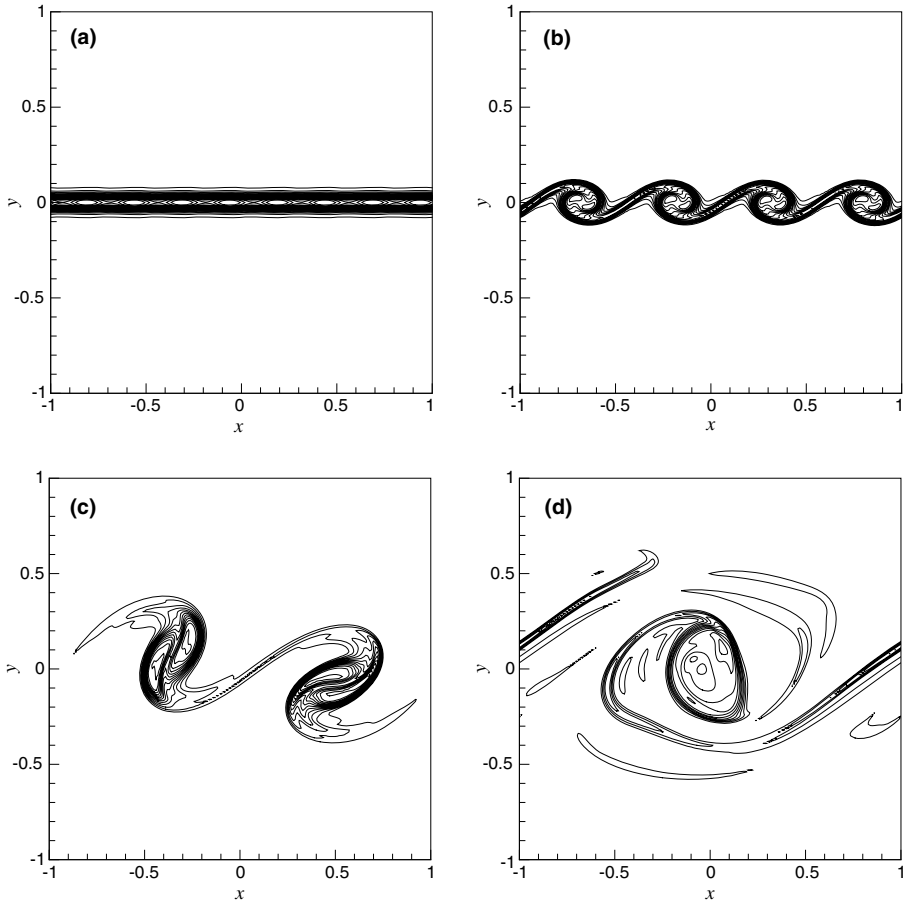

Fig. 11. Time evolution of vorticity field in the mixing layer: (a) $t = 14\delta/U_\infty$, (b) $t = 30\delta/U_\infty$, (c) $t = 60\delta/U_\infty$, (d) $t = 120\delta/U_\infty$.

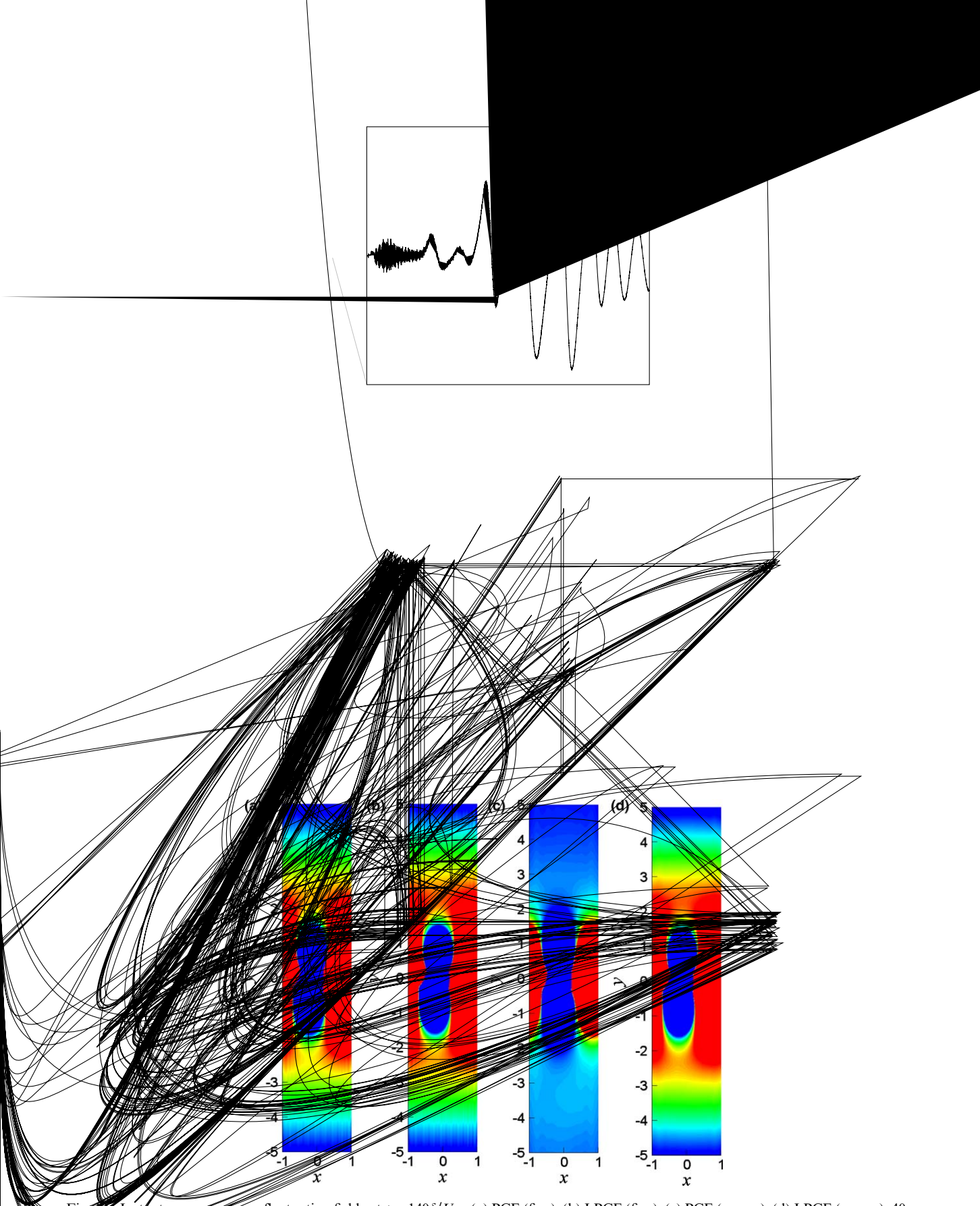

Figure 15. Instantaneous pressure fluctuation fields at $t = 140\delta/U_\infty$: (a) PCE (fine), (b) LPCE (fine), (c) PCE (coarse), (d) LPCE (coarse), 40 contour levels between -5×10^{-6} and 5×10^{-6}, non-dimensionalized by $\rho_\infty c_\infty^2$.

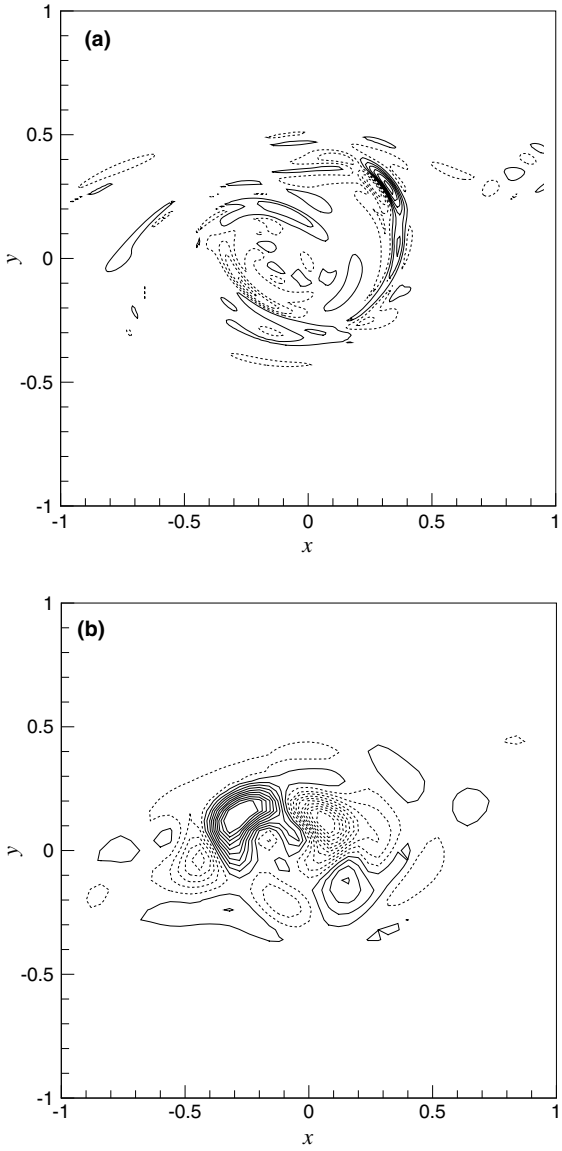

Fig. 14. Perturbed vorticity contours at $t = 140\delta/U_\infty$; calculated by PCE: (a) fine grid, (b) coarse grid, 20 contour levels between -0.4 and 0.4, non-dimensionalized by $2c_\infty/L$.

5. Conclusions

In the context of hydrodynamic/acoustic splitting method, a non-linear form of the perturbed equations allows perturbed vorticity to be generated by a coupling effect between the hydrodynamic vorticity and the perturbed velocities. At low Mach numbers, the effect of perturbed vorticity on sound generation is not significant. However, the perturbed vorticity easily becomes unstable, and causes inconsistent acoustic solutions, based on grid dependence. In the proposed linearized perturbed compressible equations (LPCE), generation of perturbed vorticity is suppressed by dropping the source terms in the perturbed vorticity transport equations. These terms are found to have a Mach number dependency $\sim O(M^4)$, whereas the leading-order terms (including the acoustic source term) are $\sim O(M)$. For various dipole and quadruple vortex-sound problems at low Mach numbers, it is successfully demonstrated that present LPCE ensures consistent, grid-independent acoustic solutions with computational efficiency.

References

[1] R. Betchov, G. Szewczyk, Stability of a shear layer between parallel streams, Physics of Fluid 6 (1963).
[2] N.B. Edgar, M.R. Visbal, A general buffer zone-type non-reflecting boundary condition for computational aeroacoustics, AIAA-Paper 2003-3300, 2003.
[3] R. Ewert, W. Schröder, Acoustic perturbation equation based on flow decomposition via source filtering, Journal of Computational Physics 188 (2003).
[4] V. Fortuné, É. Lamballais, Y. Gervais, Noise radiated by a non-isothermal, temporal mixing layer, Part I: direct computation and prediction using compressible DNS, Theoretical and Computational Fluid Dynamics 18 (2004).
[5] D. Gaitonde, J.S. Shang, J.L. Young, Practical aspects of high-order accurate finite volume schemes for electromagnetics, AIAA-Paper 97-0363, 1997.
[6] M.E. Goldstein, A generalized acoustic analogy, Journal of Fluid Mechanics 488 (2003).
[7] J.C. Hardin, D.S. Pope, An acoustic/viscous splitting technique for computational aeroacoustics, Theoretical and Computational Fluid Dynamics 18 (2004).
[8] S.K. Lele, Compact finite difference schemes with spectral-like resolution, Journal of Computational Physics 103 (1992).
[9] M. Lesieur, C. Staquet, P. Roy, P. Comte, The mixing layer and its coherence examined from the point of view of two-dimensional turbulence, Journal of Fluid Mechanics 192 (1998).
[10] A. Michalke, On the inviscid instability of the hyperbolic tangent velocity profile, Journal of Fluid Mechanics 19 (1964).
[11] Y.J. Moon, J.H. Seo, A splitting method for aeroacoustic noise prediction of low Mach number viscous flows, International Journal of Aeroacoustics 4 (1) (2005).
[12] Y.J. Moon, J.H. Seo, S.R. Koh, Y. Cho, Aeroacoustic tonal noise prediction of open cavity flows involving feedback, Computational Mechanics 31 (2003).
[13] B. Müller, On sound generation by the Kirchhoff vortex, Technical report, Uppsala University, Report No. 209, 1998.
[14] J.H. Park, C.D. Munz, Multiple pressure variables methods for fluid flow at all Mach numbers, International Journal for Numerical Methods in Fluids 49 (2005).
[15] J.H. Seo, Y.J. Moon, Perurbed compressible equations for aeroacoustic noise prediction at low Mach numbers, AIAA Journal 43 (8) (2005).
[16] J.H. Seo, Y.J. Moon, Prediction of low Mach number turbulent flow noise using the splitting method, AIAA-Paper 2004-2860, 2004.
[17] W.Z. Shen, J.N. Sorenson, Aeroacoustic modeling of low-speed flow, Theoretical and Computational Fluid Dynamics 13 (1999).
[18] S.A. Slimon, M.C. Soteriou, D.W. Davis, Computational aeroacoustics simulation using the expansion about incompressible flow approach, AIAA Journal 37 (4) (2000).
[19] S.A. Slimon, M.C. Soteriou, D.W. Davis, Development of computational aeroacustics equations for subsonic flows using a Mach number expansion approach, Journal of Computational Physics 159 (2000).
[20] M.R. Visbal, D.V. Gaitonde, High-order-accurate methods for complex unsteady subsonic flows, AIAA Journal 37 (10) (1999).